Chapter 2

Techniques and Experimental Setup

This chapter introduces the technical and experimental fundamentals of this thesis. The first two sections deal with the main surface science techniques employed in this work, i.e. Polarization Modulation Infrared Reflection-Absorption Spectroscopy (PM-IRAS) and X-Ray Photoelectron Spectroscopy (XPS).

An introduction on infrared spectroscopy will be given, and particular attention will be dedicated to describe the operational principle of PM-IRAS. The fundamentals of XPS will also be described in this chapter. As PM-IRAS study of the CO/Pd(111) system will be compared with corresponding measurements by Sum Frequency Generation (SFG) Spectroscopy (chapter 3), the basics of SFG are briefly illustrated. Methanol decomposition on Pd(111) (chapter 4) was also investigated by Scanning Tunnelling Microscopy (STM). Therefore, the principles of operation of STM will be presented as well.

Beside these methods other techniques were used: Low Energy Electron Diffraction (LEED) [15], Gas Chromatography (GC) [16], which fundamentals will not be discussed here, but described in the references. The following section describes the UHV system in which all experiments were performed. The final section describes properties, preparation and characterization of the Pd model catalysts.

2.1 PM-IRAS

As mentioned, the section dedicated to PM-IRAS begins with a general description of infrared spectroscopy and of the principles of infrared-reflection absorption spectroscopy (IRAS). Subsequently, the operation and the optical setup to perform PM-IRAS experiments will be described.

2.1.1 Introduction to Infrared Spectroscopy

Vibrational spectroscopy is one of the most important tools to investigate molecular adsorbates that form on metals in the course of surface chemical reactions. Among the different vibrational techniques, infrared spectroscopy (IR) is nowadays probably the most suitable method to study catalytically relevant adsorption systems on surfaces. In comparison with other surface techniques, such as high-resolution electron energy loss (HREELS) or Raman spectroscopy, IR spectroscopy has a high resolution (~1 cm^{-1}) and high sensitivity (typically 0.1% of a CO monolayer) and can be employed on a variety of surfaces, (from single crystals to supported catalysts and complex real catalysts), both under UHV and under more realistic pressure conditions. The principle of infrared spectroscopy is based on the vibrational excitation of molecules by absorption of infrared light. The information of these vibrational spectra is related to the chemical nature of the adsorbed molecules and also to the substrate and adsorbate-adsorbate interactions.

Fourier-Transform Infrared Spectroscopy

In the last decade, dispersive spectrometers were widely used. The frequency decomposition of polychromatic light was obtained using gratings or prisms, thus lowering the beam intensity and, consequently, increasing the acquisition time to record a spectrum with acceptable resolution and signal-to-noise ratio (S/N). Nowadays, the most frequently employed instruments are Fourier-Transform spectrometers, where all frequency components are detected simultaneously.

In FTIR-spectroscopy the interference signal of a two-beam interferometer is measured. The Michelson interferometer[1] is the heart of all modern FT-IR spectrometers. It consists of a beam splitter, a fixed mirror, and a moving mirror, as shown in Figure 2.1.

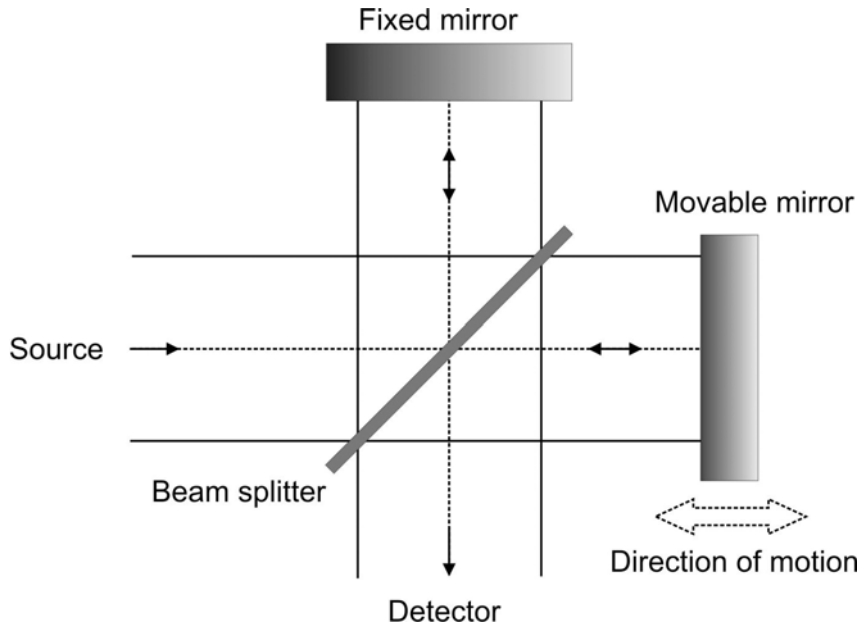

Figure 2.1: Schematic representation of the Michelson interferometer.

The collimated IR beam is partially transmitted to the moving mirror and partially reflected to the fixed mirror by the beam splitter. These two IR beams are then reflected back to the beam splitter by the mirrors. The reflected beams interfere constructively or destructively depending on the wavelength of the light and the optical path difference between the mirrors. The latter is usually referred to as retardation, δ. The resulting beam intensity $I(\delta)$, called interferogram, is measured by the detector as a function of δ. If the path difference δ is zero (the fixed and movable mirrors have the same distance from the beam splitter), constructive interference occurs, leading to a maximum in the interferogram. For all the other δ values a partial or totally destructive interference occurs, resulting in a fast oscillation decrease on both sides of the interferogram maximum (Figure 2.2a).

[1] The Michelson interferometer is a device that can divide a beam of radiation into two paths and then recombine the two beams after a path difference as been introduced. As a consequence, interference between the beams occurs.

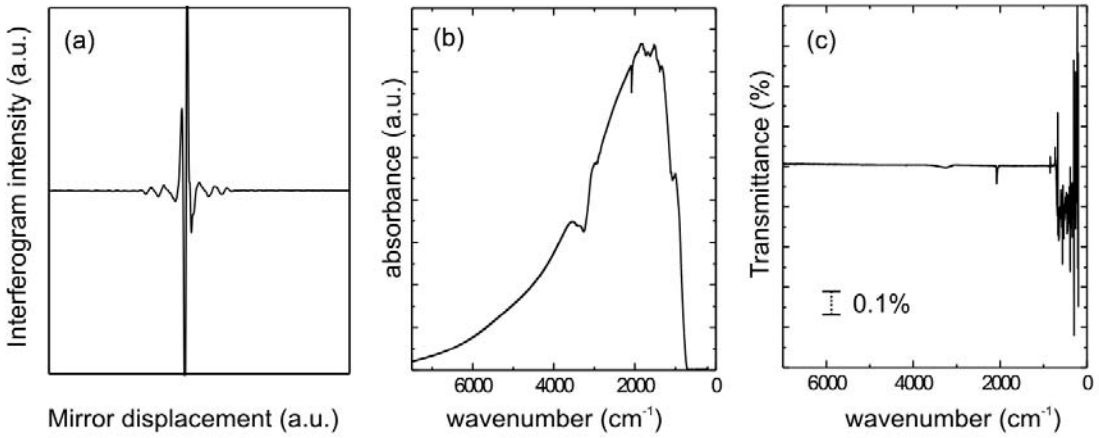

Figure 2.2: How to obtain an IR spectrum in FT-IR spectroscopy (measurement performed in the PM-IRAS setup): (a) an interferogram; (b) a single channel spectrum; (c) a transmission spectrum.

A single scan of the mirror position should be theoretically sufficient to give an interferogram, but the noise level would be high. In order to decrease it, the mirror is usually scanned N times. The interferogram $I(\delta)$ is then converted into a spectrum by computing its Fourier transform. The spectrum $S(\bar{\nu})$ describes the measured intensity as a function of wavenumber (cm^{-1}), i.e. as inverse wavelengths λ^{-1}. The spectrum $S(\bar{\nu})$, called *single channel spectrum*, is dominated by the thermal characteristics of the radiation (IR) source (globar) (Figure 2.2b). It also contains additional absorption signals due to the optical setup, the detector function and due to the molecules adsorbed on the sample. In order to retrieve only the molecular contribution (Figure 2.2c), this spectrum is divided by another single channel spectrum, obtained with the same optical setup but without adsorbates (*reference spectrum*).

It is important to notice that in a real experiment the interferogram is not a symmetric function, because of instrumental restrictions and limitations. To compensate for these limitations, different parameters are applied in the computation of the spectrum from an interferogram by the spectrometer software. For example an apodization function is introduced in order to minimize the spectral artefacts arising from that fact that the function $I(\delta)$ is measured only for finite displacements δ. For more details the reader is referred to the literature [17,18].

Infrared Reflection-Absorption Spectroscopy (IRAS)

In IRAS the vibrations of molecules adsorbed on planar surfaces, which are non transparent to the IR light, are obtained in reflection mode (Figure 2.3, left).

The vibrations *of a molecule in the gas phase* can be excited by the interaction of the electric field of incident infrared light with the dipole moment of the molecule. These vibrations are said to be infrared active, if the selection rules for electric dipole transitions are satisfied, i.e. if

$$\left(\frac{\partial \vec{\mu}}{\partial Q_k}\right) \neq 0$$

Here μ is the dipole moment and Q_k a vibrational normal coordinate. The derivative is called dynamic dipole moment of the molecule along the normal coordinate Q_k.

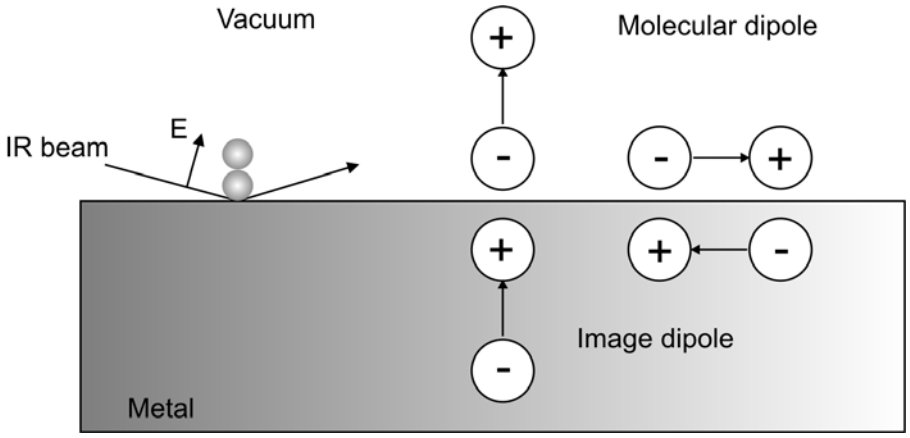

Figure 2.3: Left: IR light at grazing angle of incidence on the metal surface (indicated by a shaded block). Right: dynamic molecular and image dipoles oriented parallel and perpendicular to the metal surface.

The absorption of IR light by *a molecule adsorbed on a metal surface* is also influenced by the dielectric behaviour of the metal. On the metallic surface the electric field of the incident light and the dipole moment of the adsorbed molecule interact with the metal electrons, thus imposing a strict dipole selection rule, also known as *metal surface selection rule* (MSSR). First, only vibrations with a dynamic dipole moment component perpendicular to the surface will be excited, i.e. if

$$\left(\frac{\partial\vec{\mu}}{\partial Q_k}\right)_{\perp} \neq 0$$

The parallel component of the dynamic dipole is screened by metal electrons, which can generate an image dipole oriented opposite to those of the molecule. Figure 2.3 (right) illustrates this effect.

Second, the incident light should have a component which is p-polarized (i.e. with its electric field perpendicular to the sample surface). Accordingly to the work of Francis and Allison [19], the electric field parallel to the surface vanishes due to destructive interference. So, vibrational modes parallel to the surface cannot be excited for two reasons: there is no effective electric field parallel to the surface and because of the interaction of the molecular dipole with its image. This is why p-polarized light is used in typical IRAS experiments. Moreover, at grazing angle of incidence the phase shift and the surface intensity for p-light reach a maximum.

Summarising, the best conditions for IRAS are achieved using p-polarized light incident on the surface at a grazing angle.

Vibrational spectra of molecules in the adsorbed state are typically different from the corresponding gas-phase spectra. In fact, the observed frequencies, intensities, peak shapes and widths are influenced by the interaction between adsorbate and substrate. Nevertheless, these infrared spectra are plenty of information on the adsorption state and geometry of the molecules and their bonding to the surface. Many factors influence the spectra of adsorbed molecules and their interpretation is usually based on specific models, which can be found in [20]. Briefly, the main factors influencing the vibrational frequency of an *ensemble* of adsorbed molecules on a surface are:

a) Dynamic dipole-dipole interaction.

   When the adsorbate coverage increases, the distance among the adsorbed molecules in an adlayer decreases and thus the interaction between neighbouring dipoles and image dipoles increases (*trough space dynamic coupling*). The *coupling through metal electrons* of the substrate is another well known effect [21]. Both mechanisms induce frequency shifts towards higher wavenumbers (*blue shift*).

b) Chemical shift.

A theoretical description of the chemical shift observed for CO has been given with the backbonding model of Blyholder [22,23]. This model assumes that the bonding between CO and a metal is achieved by charge transfer from the 5σ molecular orbital (MO) of CO into the metal and by "backdonation" from metal d-bands to the unoccupied 2π* molecular orbital of CO. Since the 5σ orbital is only weakly bonding, but the 2π* orbital has a strong antibonding character, the population of the 2π*-MO weakens the CO internal bond, which corresponds to a decrease (*red shift*) in stretching frequency. With increasing coverage, adsorbate molecules compete for d-electrons from the metal orbitals, decreasing the degree of backdonation and, therefore, leading to a shift towards higher wavenumbers (blue shift).

c) Static dipole-dipole interaction.

The vibrational frequency of adsorbed molecules can be influenced by an electric field, e.g. produced by neighbouring dipoles [24]. The frequency shift of an adsorbed dipole depends on its orientation relative to the electric field it interacts with: a parallel (anti-parallel) orientation leads to a red-shift (blue-shift). This kind of contribution is typical for co-adsorption experiments where a considerably difference in the vibrational frequencies precludes dynamic dipole-dipole interactions.

2.1.2 PM-IRAS Fundamentals

IRAS is in principle not limited to low pressure. Unfortunately, in some cases it is not possible to perform high pressure studies with a conventional set up, as in the case of carbon monoxide, which is one of the most preferred probe molecules in surface science. The CO gas phase obscures the weak signal from adsorbed CO when the pressure is above 10^{-3} mbar. To exemplify that, a (standard) IRAS spectrum of 50 mbar CO adsorbed on Pd(111) at 300 K is reported in Figure 2.4. The signal from CO (linear adsorbed) around 2060 cm^{-1} is partly obscured by the rotovibrational absorption spectrum of CO gas phase.

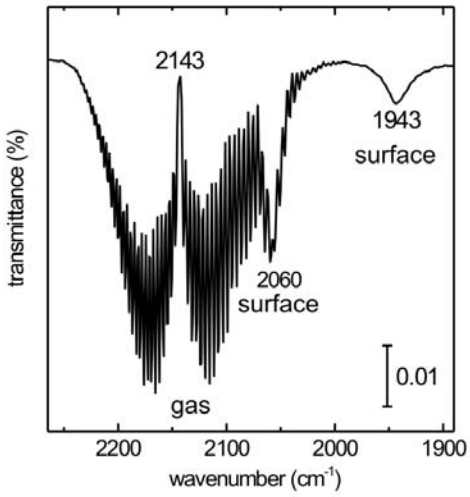

Figure 2.4: IRAS spectrum of 50 mbar CO adsorbed on Pd(111) at 300 K. The rotovibrational absorption spectrum of the gas phase obscures the signal around 2060 cm^{-1} due to adsorbed CO. The reported IRAS spectrum was measured in the PM-IRAS setup in a standard IRAS configuration.

Thus, a technique able to discriminate surface contributions from the isotropic gas phase is required to perform vibrational experiments at high pressure. This can be achieved with Polarization-Modulation IRAS (PM-IRAS). This technique has been previously used to examine surfaces in presence of liquids [25-27], and has been only recently applied to investigate model catalyst surfaces under more relevant conditions, i.e. under high pressure [10,28]. PM-IRAS was applied for the first time by *Beitel et al.* for *in-situ* investigation of gas/solid interfaces relevant to heterogeneous catalysis, i.e. CO adsorption on Co(0001) surfaces at pressure up to 600 mbar and temperatures between 300 and 550 K [29].

The polarization modulation technique is based on the modulation of a linearly polarized infrared beam, which is divided into an s-polarized beam (with its electric field parallel to the sample surface), and a p-polarized beam (with its electric field perpendicular to the sample surface). According to the metal surface selection rules discussed previously, species on a metal surface can only absorb p-polarized IR light, while molecule in an isotropic gaseous (or liquid) environment can absorb both p- and s-polarized IR light. So, it is possible to obtain a surface specific IR absorption spectrum, virtually independent of the surrounding conditions, by subtracting s-polarized absorptions from the p-polarized ones.

Normalization of this spectrum is obtained by using the total intensity of both s- and p-signals.

PM-IRAS Optical setup

The optical setup of the PM-IRAS experiment is depicted in Figure 2.5.

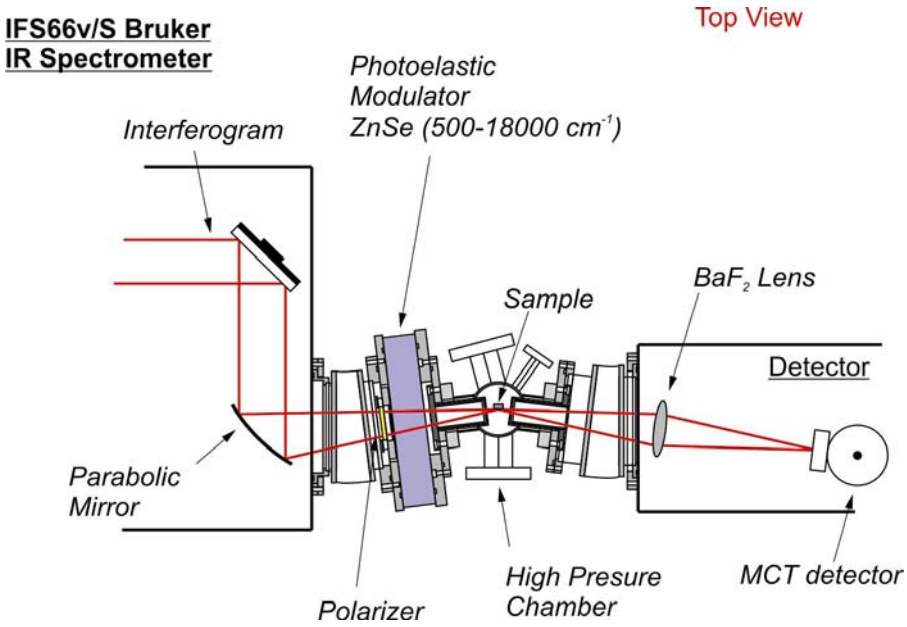

Figure 2.5: Schematic top view of the PM-IRAS optical setup.

The high-pressure cell is located between the spectrometer (IFS66v/s Bruker) and the detector chamber. Distances and angles are optimized for IRAS experiments. The spectrometer outputs a parallel IR beam of about 40 mm diameter, which is focused by a parabolic mirror (250 mm, focal length) onto the sample at an angle of 85° from the surface normal. Before entering the high pressure cell the IR beam passes through a grid polarizer so that the transmitted light has only a p-polarized electric field vector. This linearly polarized IR beam from the grid polarizer passes through a photoelastic modulator (Hinds-PEM-90 consisting of an optical element made of a ZnSe crystal, model II/ZS37, and piezoelectric transducers). The IR spectrometer and the reflected beam path are evacuated to avoid interference with atmospheric water, while the incident beam path and the PEM facilities are purged with nitrogen. After reflection from the sample, the beam is collected with a BaF_2 lens into the nitrogen-cooled MCT detector.

PM-IRAS Principles of operation

The PEM-90 principle of operation is based on the *photoelastic effect*, in which a mechanically stressed crystal exhibits birefringence proportional to the resulting strain. Different linear polarizations of light passing through a birefringent material have slightly different speeds of light. The effect of the modulator on a linear polarized monochromatic light wave is shown in Figure 2.6.

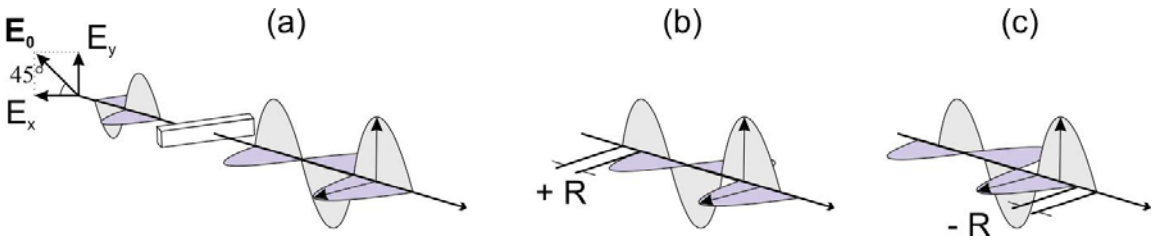

Figure 2.6: Schematic representation of the retardation effects of compression and extension of the optical element here represented in a rectangular shape. (a) Optical element relaxed. (b) Optical element compressed. (c) Optical element stressed.

When the optical element is relaxed, the light passes through it without changing its polarization (Figure 2.6a). If the optical element is compressed (Figure 2.6b), the polarization component parallel to the modulator axis travels slightly faster than the vertical component. The horizontal component than "leads" the vertical component after the light passes through the modulator. If the optical element is stretched (Figure 2.6c), the horizontal component travels slower than the vertical component. The horizontal component "lags" behind the vertical component.

The phase difference between the two components at any time is called the retardation, *R*. An important condition occurs when the peak retardation reaches one-half of the wavelength of the light (Figure 2.7a), a state which is called *half-wave retardation mode.* At the maximum of retardation, the PEM rotates the plane of polarization by 90°. Using a model II/ZS37 optical element (Figure 2.7b), the IR incoming light can be rotated by 90° with a frequency of 37 kHz and the polarization of the light impinging on the sample can be switched from p- to s-polarizations back and forth in an extremely fast way. The two states of polarization occur twice with each PEM oscillating cycle. Therefore, the sampling

frequency is 74 kHz, twice the frequency of the sinusoidal mechanical stress applied to the ZnSe crystal.

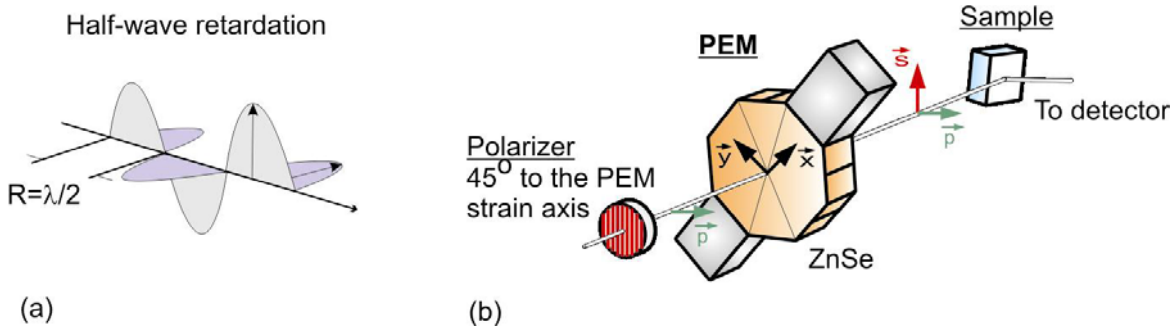

Figure 2.7: (a) Half-wave retardation. (b) Schematic representation of the optical element for PEM-90 model II/ZS37 modulator. The ZnSe crystal has an octagonal shape and a typical dark-yellow, orange colour.

The intensity of the output light after the polarization modulation can be mathematically described by a function depending on time [30]:

$$I(t) = [I_p + I_s + (I_p - I_s)\cos(\varphi_0 \cos(\gamma t))\,] / 2$$

where $I_{p,s}$ are the p- and s-polarized light intensities with respect to the sample surface, cos(γt) is set to the modulation frequency of 37 KHz, and the constant φ_0 depends linearly on the modulation voltage V_m and is inversely related to the wavelength λ of the IR light ($\varphi_0 \sim V_m / \lambda$).

To obtain the desired differential spectrum, the detector signal is processed by a specialized electronics using a single analog to digital converter (ADC), a multiplexing electronics unit (IR multiplexer), a photoelastic modulator controller (PEM 90D, Hinds Instruments) and a synchronous sampling demodulator (SSD-100, GWC Instruments). This specialized electronics generate the difference and the average interferograms, by digitizing the two signals simultaneously. In the detector signal, in fact, there are two different modulations, the *Fourier modulation* by the interferometer, and the *polarizaton modulation* by the PEM. These two modulations contain different spectral information and they have to be separated and recorded separately in order to retrieve the two spectra. The low frequency signal corresponds to the "normal" interferogram, containing the Fourier frequencies. The

high frequency signal, instead, corresponds to the PEM frequency and carries the differential absorption of s- and p-polarized light.

The detector signal is processed in the following way. The interferogram is split into two channels. In one channel the signal is passed through a low pass (LP) filter to remove the high PEM frequency. This signal, now containing only the low frequencies, is digitized and recorded to produce an interferogram. This interferogram is then transformed in a single beam spectrum of the sample, giving the average of the absorption of p- and s-polarized light by the sample. The other channel of the detector signal is processed through a synchronous demodulator (GWC Instruments), locked onto the PEM frequency. The output from this special lock-in detection is then digitized and recorded by the second digitizer. This spectrum gives the differential absorption of p- and s-polarized light by the sample.

A PM-IRAS spectrum, also called *differential reflectance spectrum* ($\Delta R/R$), is then calculated [30] from the two spectra acquired simultaneously:

$$\Delta R/R \approx [(1-\cos\varphi_0)/2 - (I_p-I_s) / ((I_p+I_s)/2) \times (\sin^2\varphi_0)/8] \times [(I_p-I_s) / ((I_p+I_s)/2)]$$

which can also be written as [30]:

$$\Delta R/R \approx J_2(\varphi_0)\,(R_p-R_s)/(R_p+R_s)$$

$J_2(\varphi_0)$ is a second order Bessel function. The $J_2(\varphi_0)$ Bessel function describes the variation of the PEM modulation efficiency with wavenumbers. The $J_2(\varphi_0)$ function gives a typical sinusoidal baseline to the spectrum which can be eliminated by dividing $\Delta R/R$ by a fitted polynomial algorithm. The differential reflectance spectrum can also be normalized by taking a background spectrum of the clean surface under identical experimental conditions. In this work all the PM-IRAS spectra reported were normalized by using background spectra of the clean sample.

For further information about the theory and the electronics involved in the PM-IRAS method for obtaining the differential reflectance spectra, the reader is referred to the literature [30,31].

2.2 X-Ray Photoelectron Spectroscopy (XPS)

Photoelectron spectroscopy (PES) is a widely used technique to investigate the electronic state and composition of a sample. It was developed in the mid 1960s by K. Siegbahn and his research group at the University of Uppsala, Sweden [32]. The phenomenon is based on the *photoelectric effect* outlined by Einstein in 1905 where the concept of the photon was used to describe the ejection of electrons from a surface when photons impinge upon it. A typical PES experimental setup is depicted in Figure 2.8a.

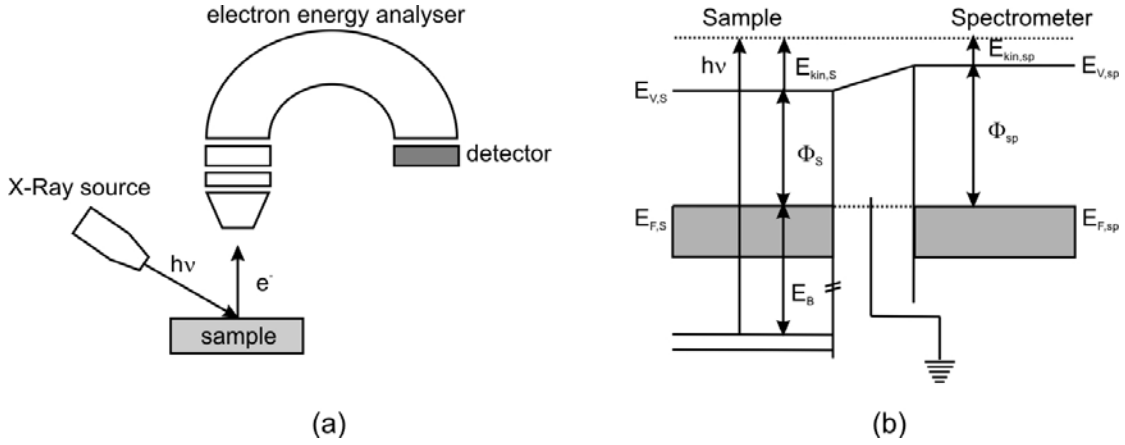

Figure 2.8: (a) Setup of a typical PES experiment. (b) Energy level diagram for the PES process.

Photons of energy $h\nu$ impinge upon a sample and cause emission of electrons which are collected by an electron lens system and subsequently detected by an energy-selective analyser. Traditionally, according to the source of excitation radiation and the energy of the excited electrons, this technique has been subdivided into ultraviolet photoelectron spectroscopy (UPS) and X-ray photoelectron spectroscopy (XPS). In UPS, valence electrons ($E < 40$ *eV*) are emitted by using UV-light (from a noble gas discharge lamp, usually a He-discharge lamp), while in XPS core level electrons ($E > 40$ *eV*) are excited using soft X-ray radiation. Frequently, for XPS a dual anode X-ray gun ($AlK\alpha$, $MgK\alpha$) is used in a common laboratory setup. The X-rays penetrate a substantial distance into the sample (~ μm), but due to the strong interaction of electrons with matter, their escape depth out of the sample is in the range of 3-30 Å, depending on their kinetic energy. That makes PES a suitable technique to probe surface electronic states of a sample [33].

The physical principles behind the photoemission process are illustrated in the energy level diagram scheme in Figure 2.8b. Conducting samples as metals are placed in electrical contact with the spectrometer, usually by simply grounding the sample and the spectrometer. Under this condition, the Fermi level of the sample and the spectrometer are at the same reference level. Accordingly, the relation governing the interaction between an impinging photon and an emitted electron can be written as

$$E_{kin,S} = h\nu - E_{b,S} - \phi_{sp}$$

where ϕ_{sp} corresponds to the work function of the spectrometer. As its value is not known, ϕ_{sp} can be calibrated by putting a standard in the spectrometer, usually a clean gold sample with a binding energy of 84.0 eV (*Au 4f*). As a result, a simple relation between the measured E_{kin} and the E_b characteristic of the sample can be obtained, as follows

$$E_{kin,S} = h\nu - E_{b,S}.$$

The different peaks in a photoelectron spectrum reflect the electronic structure of the sample. Every element has a unique set of binding energies and, therefore, an XPS spectrum gives information about the chemical composition of the sample. Moreover, it is also possible to determine the valence states of the different elements present at the surface (*chemical shift*). It is important to note that emission from non-monochromatic X-ray sources produces *satellite peaks* in the XPS spectrum appearing at lower binding energy with respect to the corresponding photoemission peaks.

The physical principles of XPS are more complicated than reported here. In fact, removing an electron from an atom causes a perturbation, leading to relaxation processes in which the remaining electrons try to screen the created hole. There are many possibilities of how the system can react to the removal of an electron, influencing differently the kinetic energy of the photoemitted electron.

For more information about the theoretical and technical description of XPS, the reader is referred to the literature [33-35].

2.3 IR-visible Sum Frequency Generation Spectroscopy (SFG)

As already mentioned in the introduction to this chapter, some measurements were performed in a different experimental setup in which SFG spectroscopy was applied (SFG experiments performed by M. Morkel). Because the SFG spectra will be discussed in the course of this thesis (chapter 3), it is worthy to briefly describe the basic principles of operation of this technique.

PM-IRAS and SFG are vibrational techniques which can detect surface adsorbate structures even in the presence of a gas phase. The fundamentals of PM-IRAS were already presented in Section 2.1.2. IR-visible sum frequency generation (IR-vis SFG) spectroscopy is a nonlinear optical technique which provides vibrational spectra of molecules adsorbed on a surface while the molecules in the gas phase do not produce any signal. Therefore, SFG can be applied from UHV up to elevated pressure on molecules adsorbed on different substrates, such as single crystals, thin films, metal foil and supported nanoparticles.

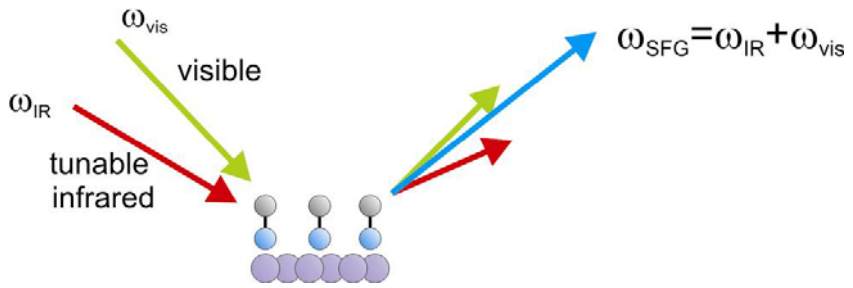

Figure 2.9: Schematic representation of the IR-vis sum frequency generation (SFG) process.

Picosecond laser pulses at a tunable infrared frequency ω_{IR} and at a fixed visible frequency ω_{vis} are spatially and temporally overlapped on the sample surface. The tunable pulse in the mid-IR range (ω_{IR}) allows probing the vibrational modes of adsorbed surface species. A sum frequency signal ($\omega_{SFG} = \omega_{IR} + \omega_{vis}$) is generated due to a second-order non-linear optical process. In a very simple representation, this signal is considerably enhanced when the IR frequency coincides with an adsorbate vibrational resonance. By tuning the IR beam and monitoring the intensity of the SFG output, a vibrational spectrum of the adsorbed species is obtained by plotting the SFG intensity vs. the IR wavenumber. Because

SFG is not allowed in media with inversion symmetry, the SFG signal is mainly generated by the adsorbed molecules, whereas the centrosymmetric bulk of the metal and the isotropic gas phase give only a small contribution to the signal. Therefore, SFG is an inherent surface sensitive technique which can be applied from UHV up to high pressure conditions.

For further details about SFG spectroscopy the reader is referred to the literature [36,37].

2.4 Scanning Tunneling Microscopy (STM)

The scanning tunneling microscope (STM) was invented in 1981 by G. Binnig and H. Rohrer of IBM's Zurich Lab in Zurich, Switzerland. G. Binnig and H. Rohrer won the Nobel Prize in Physics in 1986 for development of this technique (together with E. Ruska). The STM is a non-optical microscope which is applied to probe local areas of conducting surfaces on a nanometer scale. Topographical[2] information and the electronic structure of the surface can be obtained [38].

A schematic drawing of a typical STM setup is shown in Figure 2.10.

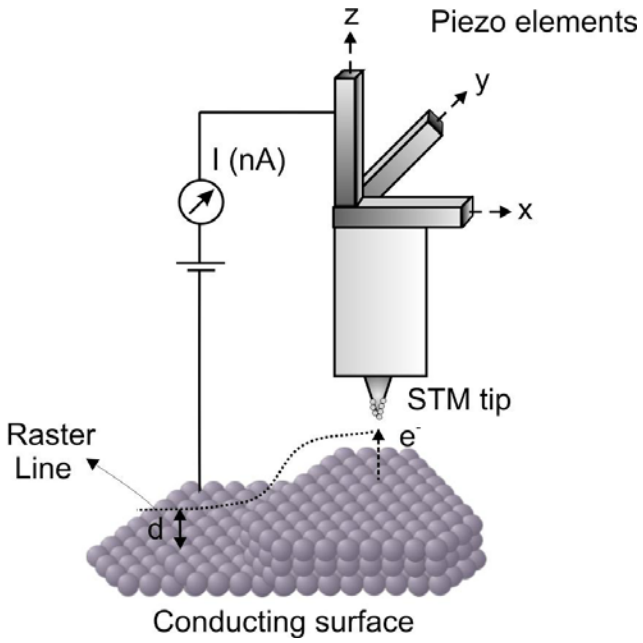

Figure 2.10: Schematic drawing of a typical STM setup representing tunnelling of the electrons from the sample to the positively biased STM tip. The quantity d is the sample-tip separation.

[2] The contrast in an STM image reflects the contour of the local density of electron states. Only under special conditions the contrast of an STM image reflects exclusively the topographic properties of the surface.

In STM, a sharp metal tip (usually Tungsten or Pt-Ir) is placed within a few Å above the surface of a conducting sample. At this close distance, the electronic states of the tip and the sample surface start to interact. If a bias voltage (U) is applied between the tip and the sample surface, it is probable that electrons will cross the vacuum barrier separating them. Depending on the applied voltage, the electrons can tunnel from the tip to the sample surface and viceversa. If a small positive bias is applied to the tip, its Fermi level (E_F) will be lower than that of the sample, and thus electrons from the occupied states that are close to the E_F of the metal (sample) will tunnel through the vacuum to fill the empty states of the tip. A tunneling current (I) is created that can vary from pico- to nano-ampers. The tunneling current is exponentially depending on the distance d between the tip and the sample [38]. Therefore, information about the topology of the sample can be obtained by measuring I on the sample surface.

In a similar way, if a negative bias is applied to the tip, tunneling from occupied tip states to the empty electronic states of the sample occurs, enabling the investigation of the unoccupied density states of the sample surface.

In order to get a two-dimensional image of the sample, the tip is scanned over its surface by means of piezoelectric elements. STM experiments can be performed in two different modes called *constant current* and *constant height modes*. In the constant current mode a feedback mechanism adjusts the height of the tip during scanning so that the tunnelling current flowing between tip and sample is kept constant. In the constant height mode, also called “variable current” mode, the tunnelling current changes according to the protrusion on the surface.

The STM measurements reported in chapter 4 were performed in a different apparatus at the Fritz-Haber-Institute, in cooperation with S. Guimond. This experimental setup is an Omicron system with facilities to perform LEED, XPS and room temperature STM. Pt-Ir tips were used to acquire STM images in UHV (base pressure below $1x10^{-10}$ mbar) in the constant current mode. For more details about the Omicron experimental setup the reader is referred to [39].

2.5 The Ultra High Vacuum System

The first challenges during this work were to complete the installation of the UHV-system sketched in Figure 2.11 and to test its applicability to study heterogeneous catalytic systems. Most of the experiments presented in this thesis were performed in the so called "PM-IRAS" setup (Fig. 2.11), in which both sample preparation and characterization can be carried out within one vacuum system. The equipment combines a UHV preparation chamber with a UHV-high pressure cell optimized for the PM-IRAS geometry and for performing kinetic measurements by means of GC.

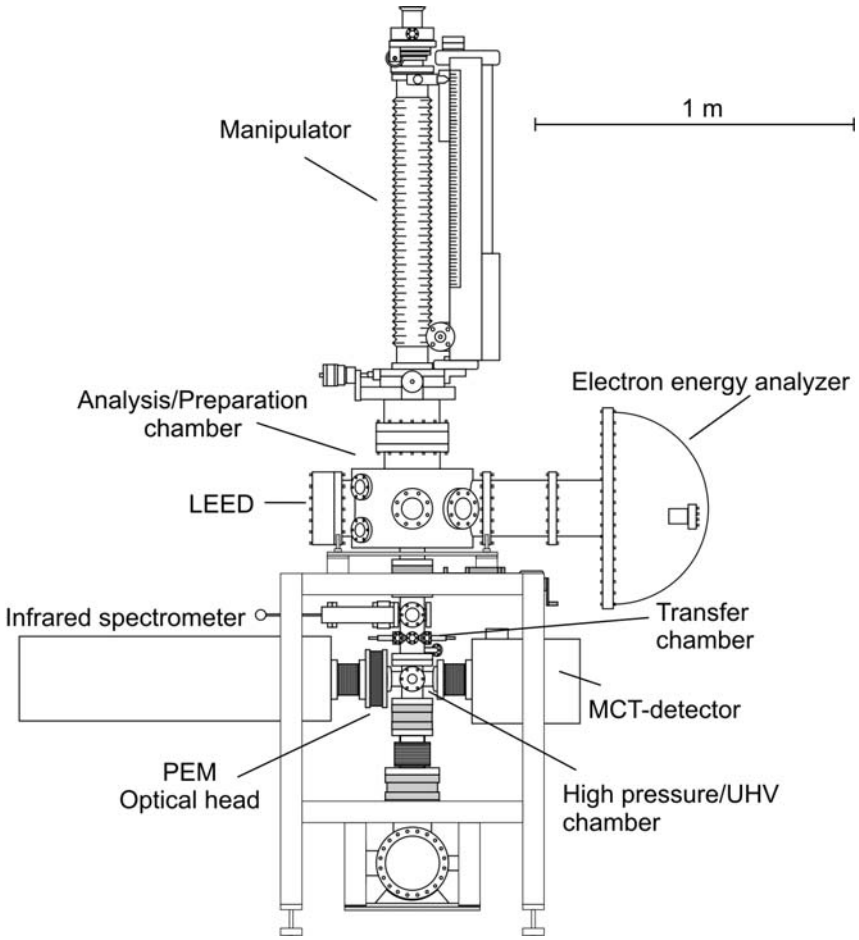

Figure 2.11: Schematic illustration (front view) of the UHV-system including the most important sections.

The preparation chamber is equipped with a sputter gun, a quartz balance, a single electron beam evaporator, a mass spectrometer, a four-grid LEED optics and facilities for XPS experiments. These consist of a hemispherical electron energy analyser (SPECS

PHOIBOS 150) and a dual anode X-ray gun (SPECS XR50) emitting $AlK\alpha$ and $MgK\alpha$ radiation (non-monochromatic). Gases can be dosed in the chamber through a leak valve. The chamber is pumped through a turbomolecular pump, which ensures a base pressure below $5x10^{-10}$ mbar during routine operation (< $2x10^{-10}$ after bakeout), monitored by an ionization gauge. The values for the different dosed gases are given taking into account the relative sensitivity factors [40,41]. The rate of evaporation of the electron beam evaporator is calibrated using the quartz balance.

The sample is mounted in a Tantalum-wire grid, which is spot welded to two Molybdenum rods. These rods are fixed in a cold-finger connected to the manipulator, allowing free motion of the sample in the x, y, z, ϕ directions. Temperature reading is made via a type K thermocouple (made of a positive Chromel wire and a negative Alumel wire), spot welded to the rear of the crystal. The sample can be resistively heated up to 1300 K and cooled down to 90 K introducing liquid nitrogen in the cold-finger. The surface cleanliness can be checked with XPS and TDS analysis. LEED analysis gives information about surface structures.

For vibrational studies, the sample is moved to the UHV-high pressure chamber with the manipulator. During the transfer, the sample holder is introduced into differentially pumped Teflon seals, thus separating the UHV upper chamber from the high pressure section during PM-IRAS (and GC) experiments. Under UHV- and HP-conditions, the lower chamber is pumped down by a turbomolecular pump, which can be separated by a manually operated gate valve during high pressure experiments.

The high pressure chamber is supplied with CaF_2 windows for IR experiments and is gold coated to minimize background activity. The instrument used in this work is a FT-IR spectrometer from Bruker (IFS66v/S), equipped with a thermal radiation source (Globar: silicon carbide) and a $l\text{-}N_2$ cooled MCT (Mercury-Cadmium-Telluride) detector. A metal grid polarizer, a photoelastic modulator (Hinds-PEM-90), a ZnSe collector lens and an electronic demodulator are other elements necessary for the PM-IRAS experiments

The used gases have the following purity: CO (99,997%), H_2 (99,99990%), Ar (99,99990%), O_2 (99,9995%), C_2H_4 (99,95%), C_4H_6 (99+%). During high pressure experiments, great care has to be taken to control CO cleanliness, in order to prevent Ni

surface contamination coming from the dissociation of Ni- and Fe-carbonyls [42,43]. For the experiments presented in this work, the impurities were removed by passing CO over a carbonyl absorber cartridge and a cold trap filled with liquid nitrogen. Methanol (purity: 99.9%) was purified using repeated freeze-pump-thaw cycles.

2.6 Pd model catalysts

In this work two model catalysts were used, Pd(111) single crystal and Pd-nanoparticles supported on alumina.

At the beginning of the experimental work, the test and start up of the new PM-IRAS experimental setup were required. Experiments were first carried out on a more simple system, i.e. Pd(111). At the beginning, UHV and high-pressure measurements were performed dosing a simple probe molecule, CO, on Pd(111). Subsequently, the interaction of more complex molecules on the Pd(111) surface was studied. Initial work on catalytically more relevant systems, such as Pd supported nanoparticles, will also be discussed.

Pd (111)

The Pd(111) single crystal has the shape of a disc of 8-10 mm diameter and of 2-4 mm thickness. Before mounting it in the UHV system, it was cut and polished following the standard procedure. Its orientation was checked by X-ray diffraction and the maximum accepted angular deviation is below 0.5°. The sample is first heated to 1250 K, and then Ar^+-sputtered at room temperature for 30-45 min at an Argon pressure of $5x10^{-6}$ mbar and a sputtering current of ~5 μA, subsequently annealed to 1250 K and oxidized in $5x10^{-7}$ mbar O_2 from 1200 K to 600 K, and finally flashed to 1200 K to remove the adsorbed oxygen species. The morphology and the degree of surface cleanliness can be checked by LEED and XPS, as shown in Figure 2.12 for a clean sample.

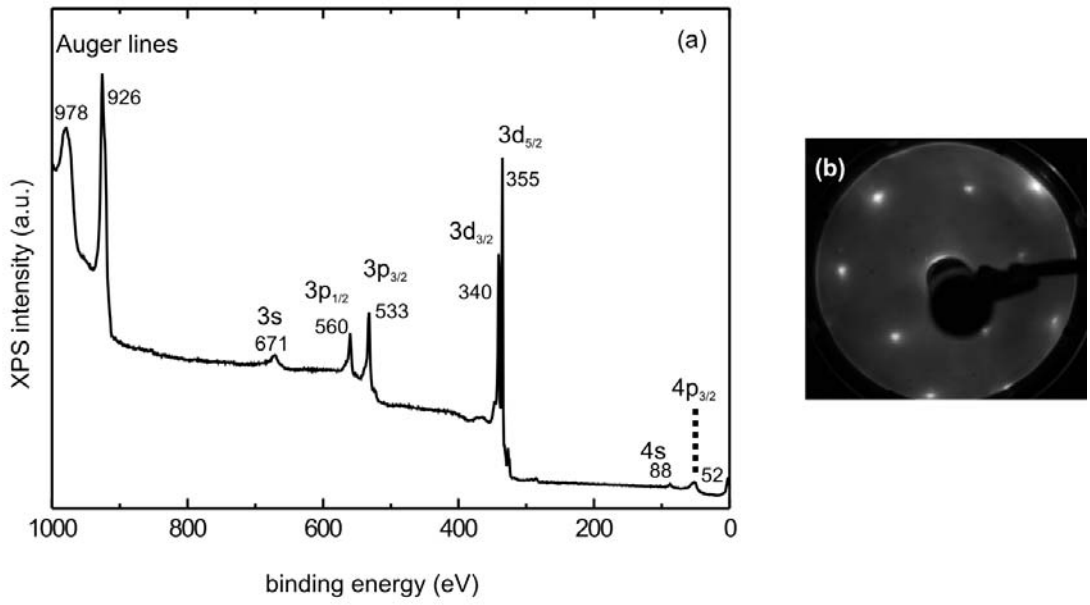

Figure 2.12: (a) XPS spectrum of a freshly prepared Pd(111) surface taken with *MgKα* radiation at normal emission. The main core level and Auger peaks are also indicated. (b) LEED pattern with hexagonal symmetry (E_{el} = 90 eV).

A recent STM study [44] has shown the presence of three distinct types of subsurface impurities in Pd(111), which were assigned to S, C, and O. Because of their low concentration, these subsurface impurities could only be detected by STM.

$Pd/Al_2O_3/NiAl(110)$

Metal-nanoparticles supported on alumina are frequently used in heterogeneous catalysis [45]. In our department the $Pd/Al_2O_3/NiAl(110)$ model catalyst was characterized by many surface science technique (XPS, TDS, HREELS, IRAS, STM, AFM). A few Å thick alumina film is prepared by oxidation of a NiAl(110) single crystal, and the Pd particles are grown on the support by metal vapour deposition. First, the NiAl(110) surface is cleaned by several cycles of Ar^+ sputtering (1 KeV, ~4 mA, 45 min) at 780 K followed by annealing to 1300 K for 5 minutes in order to restore the initial stoichiometry. The surface is then oxidized in $1x10^{-6}$ mbar O_2 at 550 K and then annealed at 1050 K. This

oxidation/annealing cycle is repeated twice. The alumina film obtained is stable up to a temperature of 1150 K. It is atomically flat and has a thickness of about 5 Å [46], which corresponds to approximately two Al-O layers. More details about alumina properties and its structure can be found in the references [47-50]. Typical LEED patterns of NiAl(110) and of the aluminium oxide film are shown in Figure 2.13a and Figure 2.13b, respectively. XPS spectra of the alumina film are also reported. In Figure 2.13c an overview scan of the alumina film is reported, showing the main core level and Auger signals. The *O1s* peak (Figure 2.13d) is centred at 531.5 eV and exhibits a shoulder towards higher binding energy, probably related to oxygen ions in the topmost layer of the film. The close-up in the *Al2p* region (Figure 2.13e) shows a predominant feature due to aluminium in a metallic environment (NiAl, ~72.5 eV), and a pronounced shoulder at higher binding energy due to the oxidation of aluminium (Al_2O_3, ~75.5 eV).

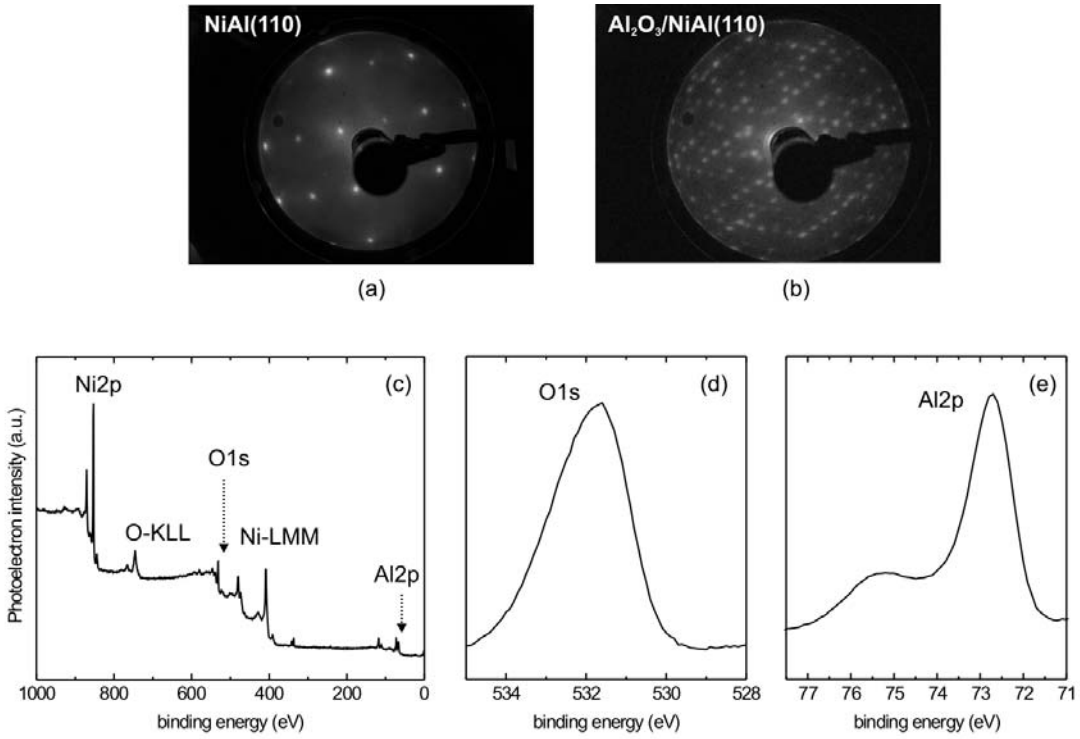

Figure 2.13: (a) LEED pattern of NiAl(110) substrate before the oxidation. (b) LEED pattern of a high ordered Al_2O_3-film (E_{el} = 80 V). Low: XPS spectra of the alumina film taken with *MgKα* radiation at normal emission. (c) Overview scan, (d) *O1s* region, (e) *Al2p* region.

From STM images, it is evident that the alumina film exhibits a number of characteristic defects, arising form the coexistence of two reflection domains as well as

from the slight mismatch between the substrate and the film. There are line defects between the two different Al_2O_3-domains and antiphase domain boundaries between domains of the same orientation, and point defects, which are possibly oxygen vacancies. For the nucleation of the deposited metal particles, the line defects play a crucial role. The nucleation behaviour of metals on the thin alumina film depends also on the temperature of the substrate [51].

Palladium is deposited on alumina by evaporation from a rod (diameter: 1 mm, purity > 99,99%), by electron bombardment heating[3]. The sample and the evaporator are kept at the same potential of 800 V, in order to deposit on the film only single, neutral Pd atoms without degradation of the Al_2O_3-support. The nucleation starts on the line defects if the sample is kept at 300 K, and additional Pd atoms start to grow on these nuclei. Depending on the absolute amount of Pd deposited, it is possible to obtain particles with different sizes (from 1 nm to 10 nm). It is possible to grow more defective clusters if the sample is kept at 90 K. At this temperature the mobility of the metal atoms is lower, thus Pd nucleates primarily at point defects.

The Pd particles of this work were deposited on the alumina film by evaporation of nominally 6 Å Pd at 300 K. The average size of each particle is 6 nm, made of ~4000 atoms. The shape of these three-dimensional particles is well defined, i.e. truncated cubo-octahedrons are formed. The crystalline particles grow preferentially in (111) orientation and exhibit predominantly (111) facets as well as small fraction of (100) facets (see Figure 2.14).

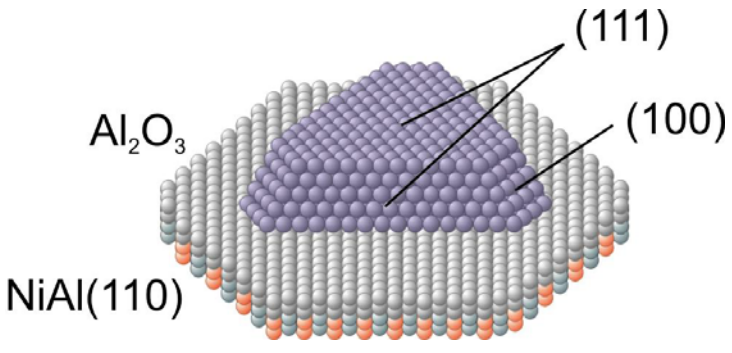

Figure 2.14: Model of Pd/Al_2O_3 system.

[3] The bombarding electron beam induces a temperature rise of the evaporant, causing evaporation.

Pd particles freshly prepared on the alumina film undergo a stabilization procedure, which can prevent structural properties changes during catalytic reactions. Their thermal stability is increased up to at least 500 K. The stabilization procedure consists of an extended oxygen exposure ($1x10^{-6}$ mbar O_2) at 500 K, followed by CO exposure to react away the remaining oxygen adsorbed atoms by desorbing CO_2. The adsorbed CO is thermally desorbed. By this procedure, the oxide layer thickness is increased [52].

Further information on the $Pd/Al_2O_3/NiAl(110)$ system can be found in [53-55].